

T. J. Hobbs

Phenomenological implications of the nucleon's meson cloud

Received: date / Accepted: date

Abstract The long-distance structure of the interacting nucleon receives important contributions from its couplings to light hadronic degrees of freedom — a light meson cloud — while an analogous nonperturbative mechanism is expected to generate an intrinsic charm (IC) component to the proton wavefunction. We investigate both possibilities, keeping for the former a special eye to improving the theoretical understanding of the pion-nucleon vertex in light of proposed measurements. Regarding the latter possibility of IC, we highlight recent results obtained by a global QCD analysis of the light-front model proposed in Ref. [1].

Keywords quark models · heavy quarks · effective field theory · deeply inelastic scattering

1 Introduction

As much as a desire to understand bound state properties of hadrons motivated the development of QCD, efforts based solely upon perturbative QCD remain stubbornly unyielding toward a thorough grasp of long-range hadronic structure. The defining reason has much to do with the fact that nonperturbative mechanisms are decisive in shaping various aspects of the makeup and internal dynamics of hadrons. That this must be the case is evident, for instance, in the role played by light pionic modes in qualitatively shaping the peripheral charge distribution of the nucleon due to pion-nucleon loop corrections at its electromagnetic vertex. Such corrections are a direct consequence of the nucleon's *pion cloud* — essentially, a dressing of the nucleon wavefunction by short-lived configurations of virtual $SU(2)$ mesons, of which the pion as the lightest mode is expected to dominate at small momenta ($\lesssim 500$ MeV). In fact, at small values of the t -channel exchange mass ($t \sim m_\pi^2$) the presence of the pion cloud provides a natural description of the electron-nucleon DIS interaction in terms of spontaneous dissociations of the form $N \rightarrow \pi N$ under the constraints of, *e.g.*, charge conservation and gauge invariance.

The existence of the pion cloud is in principle well-established by a substantial body of experimental measurements and theoretical analyses (*e.g.*, of light quark sea asymmetries $[\bar{u} - \bar{d}](x) \neq 0$ relevant to Gottfried Sum Rule violation [2]). At the same time, the detailed momentum dependence of the pion-nucleon vertex remains a significant source of model dependence in any effort at first-principles calculation; proposed DIS extractions of the pion structure function (SF) $F_2^\pi(x, Q^2)$ at the crucial pion mass pole $t = m_\pi^2$ depend upon sensitivity to mechanisms including those depicted in Fig. 1 for which

This material is based upon work supported by the U.S. Department of Energy Office of Science, Office of Basic Energy Sciences program under Award Number DE-FG02-97ER-41014. NT@UW-14-24.

T. J. Hobbs
Department of Physics, University of Washington, Seattle, WA 98195-1560
Tel.: +1-206-543-9754
E-mail: tjhobbs@uw.edu

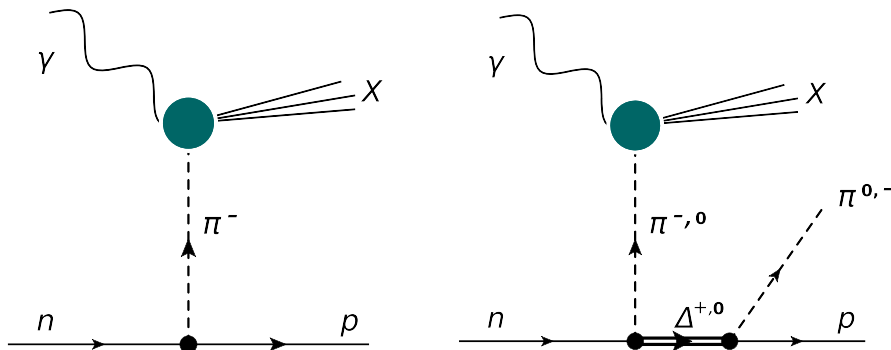


Fig. 1 We take the dominant process to be light meson exchange as typified by these one-pion graphs; the effects of intermediate Δ states are also considered numerically.

systematic estimations at the relevant kinematics remain lacking — an issue we explore in Sec. 2 in light of the experimental possibility of forward spectator tagging [3]. On the other hand, though the validity of the “cloud” picture might break down with increasing mass, the basic meson-baryon Fock state ansatz also remains a sensible means of determining nonperturbative contributions from heavy quarks [1], as we highlight with a summary of a related QCD global fit in Sec. 3.

2 Pion-nucleon interactions and spectator tagging

To lowest order, the process of Fig. 1 implies a two-component Fock state expansion of the type

$$|N\rangle = \sqrt{Z_2} |N\rangle_0 + \sum_{M,B} \int dz f_{MB}(z) |M(z); B(1-z)\rangle, \quad (1)$$

where for full generality, the wavefunction of the physical nucleon is taken to be a direct sum of a renormalized bare term with a contribution from meson-baryon virtual states. The meson-baryon splitting function $f_{MB}(z) = \int dk_{\perp}^2 \phi_{MB}(z, k_{\perp}^2)$ requires the computation of the amplitudes $\phi_{MB}(z, k_{\perp}^2)$, which we undertake on the light-front in terms of the momentum fraction $z = k^+/P^+$ of the intermediate meson with respect to the initial state nucleon. Fortunately, χ Pt provides the necessary lagrangians to satisfy gauge invariance, and for the pion sector we take the relevant interaction to be

$$\mathcal{L}_{\pi N} = \frac{g_A}{2f_{\pi}} \bar{\psi}_N \gamma^{\mu} \gamma_5 \boldsymbol{\tau} \cdot \partial_{\mu} \boldsymbol{\pi} \psi_N - \frac{1}{(2f_{\pi})^2} \bar{\psi}_N \gamma^{\mu} \boldsymbol{\tau} \cdot (\boldsymbol{\pi} \times \partial_{\mu} \boldsymbol{\pi}) \psi_N, \quad (2)$$

in which the leading term in Eq. (2) induces characteristic “rainbow” graphs whence the pionic $\phi_{MB}(z, k_{\perp}^2)$ may be derived, and the second, Weinberg-Tomozawa term does not contribute to the present analysis. Following a standard process for the pseudoscalar pion, one may obtain

$$f_{\pi N}(z) = c_I \frac{g_{\pi NN}^2}{16\pi^2} \int_0^{\infty} \frac{dk_{\perp}^2}{(1-z)z(M^2 - s_{\pi N})^2} \left(\frac{k_{\perp}^2 + z^2 M^2}{1-z} \right), \quad (3)$$

where k_{\perp} is the transverse momentum of the exchanged pion in the Sullivan process of Fig. 1, $g_{\pi NN}$ is the well-known πNN coupling constant, M the nucleon mass, and the isospin factors for the individual charge states are $c_I = 1$ for π^0 ($p \rightarrow p\pi^0$ or $n \rightarrow n\pi^0$) and $c_I = 2$ for π^{\pm} ($p \rightarrow n\pi^+$ or $n \rightarrow p\pi^-$). While the spin-structure and general form of Eq. (3) are fully determined diagrammatically, the UV-divergent behavior that originates with the implicit k_{\perp}^2 integration of Eq. (1) is a primary source of model dependence, with a variety of phenomenological form factors traditionally used to control the irregular behavior at large momenta; here we make use of an s -dependent scheme: $G_{\pi N} = \exp[(M^2 - s_{\pi N})/\Lambda^2]$.

With these, as well as corresponding expressions for other $SU(2)$ processes involving scattering from the ρ or intermediate Δ exchanges, etc., we are in a position to make definite predictions for experimental observables, including meson cloud components of DIS structure functions. In keeping with the current model uncertainties regarding the pion-nucleon vertex described at the outset of the

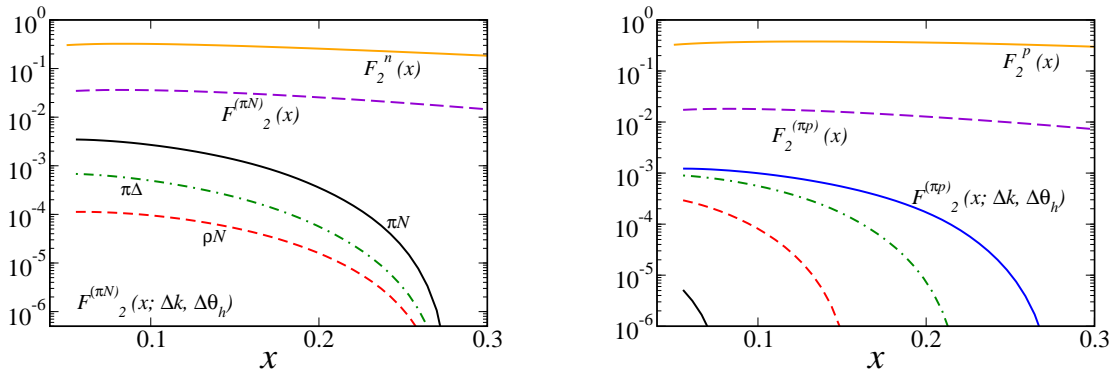


Fig. 2 Contributions from tagged structure functions for various hadronic species (left), and for various integration ranges in the final state momentum $\Delta|\mathbf{k}|$ (right) as determined by Eq. (7) and explained in-text.

present note, it would be particularly helpful for experiments to measure the momentum dependence of contributions from the processes depicted in Fig. 1. In practice, this might best be achieved via an experimental program to systematically “tag” produced baryons as well as carefully measure their final-state momentum with sufficiently sensitive forward calorimetry. With the resulting information, one could then deduce on the basis of momentum conservation the kinematics of the one-boson exchanges shown in Fig. 1, and thereby constrain models of the type specified by Eq. (3).

Thus, with explicit calculations for the pion-nucleon distribution amplitudes, (*e.g.*, Eq. [3]), we can write the fully inclusive contribution of the pion sector to the DIS structure function of the nucleon:

$$F_2^{(\pi N)}(x) = \int_x^1 dz f_{\pi N}(z) F_{2\pi}\left(\frac{x}{z}\right); \quad (4)$$

we will find it useful to recast this in terms of lab-frame variables,

$$\begin{aligned} \tilde{z} &= \left(k_0 + |\mathbf{k}| \cos \theta_{p'}\right) / M, & \tilde{k}_\perp &= |\mathbf{k}| \sin \theta_{p'} \\ k_0 &= M - \sqrt{M^2 + \mathbf{k}^2}, \end{aligned} \quad (5)$$

where $|\mathbf{k}|$ is the deposited three-momentum of the final-state baryon, unobserved in the inclusive process implied by Eq. (4), and $\theta_{p'}$ is its laboratory angle relative to the longitudinal direction defined by an incident photon. In contrast to these inclusive considerations, a detailed mapping of the momentum dependence of one-pion exchange in DIS requires a careful binning of the contributions embodied by Eq. (4) in finite ranges of the transverse momentum $k_\perp^2 \in \Delta k_\perp^2$ and fraction $z \in \Delta z$ (using the “natural” parametrization of the pion cloud). The resulting “tagged structure functions” are then specified as

$$F_2^{(\pi N)}(x, \Delta z, \Delta k_\perp^2) = \frac{1}{M^2} \int_{\Delta z} dz \int_{\Delta k_\perp^2} dk_\perp^2 f_{\pi N}(z, k_\perp) F_{2\pi}\left(\frac{x}{z}\right), \quad (6)$$

in which the factor of M^{-2} is present to preserve the dimensionlessness of the integral.

Keeping with the expressions of Eq. (5), it is useful to render tagged SFs in the appropriate laboratory kinematics — *i.e.*, the three-momentum of the produced baryon $|\mathbf{k}|$ and its laboratory angle $\theta_{p'}$. Evaluating in terms of the lab-frame definitions \tilde{z} , \tilde{k}_\perp , we obtain

$$F_2^{(\pi N)}(x, \Delta|\mathbf{k}|, \Delta\theta_{p'}) = \frac{1}{M^2} \int_{\Delta|\mathbf{k}|} d|\mathbf{k}| \int_{\Delta\theta_{p'}} d\theta_{p'} J(x, |\mathbf{k}|, \theta_{p'}) f_{\pi N}(\tilde{z}, \tilde{k}_\perp) F_{2\pi}\left(\frac{x}{\tilde{z}}\right), \quad (7)$$

and, much as before, $\Delta|\mathbf{k}|$, $\Delta\theta_{p'}$ denote finite integration ranges determined by experimental resolution; the quantity $J(x, |\mathbf{k}|, \theta_{p'})$ is the Jacobian associated with the transformation from the “theory” space

relevant for Eq. (6) to the lab-frame parametrization used above. Explicitly,

$$\begin{aligned} J(x, |\mathbf{k}|, \theta_{p'}) &= \frac{\partial(x, \tilde{z}, \tilde{k}_\perp^2)}{\partial(x, |\mathbf{k}|, \theta_{p'})} \\ &= \frac{2}{M} |\mathbf{k}|^2 \sin \theta_{p'} (1 - \sin \phi_k \cos \theta_{p'}) . \end{aligned} \quad (8)$$

where we have defined $\phi_k = \tan^{-1}(|\mathbf{k}|/M)$.

Using lagrangians similar to Eq. (2), one may compute probability distributions analogous to Eq. (3) for ρ exchange and Δ recoils — *i.e.*, $f_{\rho N}(z)$, $f_{\pi\Delta}(z)$ [4] — and use the formalism summarized by Eqs. (4)–(8) to determine their contributions to the tagged F_2 structure function. As an illustration, one might assume the experimental range of the proposed JLab Hall A measurements described in Ref. [3]. Here, the drive is to probe softer exchanges (*i.e.*, near the $t = m_\pi^2$ pion pole), and we therefore integrate over the modest range $\Delta|\mathbf{k}| = [250, 400 \text{ MeV}]$, and include all accessible baryon production angles in the left panel of Fig. 2. At such small momenta, the contributions to $F_2^{(\pi N)}(x, \Delta|\mathbf{k}|, \Delta\theta_{p'})$ from single pion exchange dominate other mechanisms (which possess more nonlinear momentum dependences) by an approximate order-of-magnitude.

The observed level of separation among the various $SU(2)$ processes in the tagged structure functions implies that a more sensitive unraveling of the pion Sullivan process may be achievable; to that end, the detailed momentum dependence of this latter process is depicted in the right-hand side of Fig. 2. Presuming a high degree of resolution in $|\mathbf{k}|$, the RHS of Fig. 2 renders the single neutral-pion exchange contributions to F_2 as given by Eq. (7) in fine windows of $\Delta|\mathbf{k}| = [0.06, 0.1]$, $[0.1-0.2]$, $[0.2-0.3]$, and $[0.3-0.4 \text{ GeV}]$ — going respectively from the solid black to solid blue curves. As in the left panel of Fig. 2, the fully integrated πN contributions (violet, dashed — given by Eq. [4]) and full DIS structure functions (either F_2^n or F_2^p , in solid orange) are given for comparison.

In particular, there is again a fairly marked separation, this time in $\Delta|\mathbf{k}|$ due to momentum tagging of the forward spectator baryon. With sensitivity to tagged SFs/fracture functions at the level of $\sim 4 \times 10^{-5}$ as might be provided by the upgraded Hall A projection chamber [3], careful measurement could in fact better elucidate the πN vertex, whose description remains heavily model-dependent, but nonetheless explicitly controls the Sullivan process of Fig. 1. These phenomenological improvements would of course also enhance the understanding of the pion structure function F_2^π itself, as well as yield unprecedented information near the pion's physical pole.

3 Global analysis of intrinsic charm

While the meson cloud is especially adapted to the light sector — where chiral symmetry breaking provides physical motivation for the pion cloud picture of nucleon structure — Eq. (1) is sufficiently general to allow an extension of the preceding formalism to heavier mass scales. In fact, an extension of this type might serve as the basis for an investigation of the contributions to nucleon structure due to nonperturbative heavy quarks, including *intrinsic* charm (IC) [5].

In Ref. [1], precisely such an analysis was explored, with the end result being a two-step calculation yielding non-zero IC PDFs of the form

$$c(x) = \sum_{B,M} \left[\int_x^1 \frac{d\bar{z}}{\bar{z}} f_{BM}(\bar{z}) c_B\left(\frac{x}{\bar{z}}\right) \right], \quad \bar{c}(x) = \sum_{M,B} \left[\int_x^1 \frac{dz}{z} f_{MB}(z) \bar{c}_M\left(\frac{x}{z}\right) \right], \quad (9)$$

where $\bar{z} = 1 - z$, and z retains its definition as given in Sec. 2. In contrast to the foregoing analysis, the sums over (B, M) of Eq. (9) now involve (anti-)charm-containing $SU(4)$ hadrons, and the hadronic splitting functions $f_{MB}(z)$ must be evaluated using a hadronic effective theory. It is of course also necessary to determine the intermediate distributions $c_B(x/\bar{z})$ and $\bar{c}_M(x/z)$, which were computed using a simple relativistic quark model formulated on the light front as detailed in [1].

With our framework, one may then incorporate intrinsic charm at the partonic threshold $Q^2 = m_c^2 \sim 1.69 \text{ GeV}^2$ and investigate implications for higher energy data using standard QCD evolution and the various IC model prescriptions treated in [1]; doing so, it was found that hadroproduction data might serve to constrain the model parameters that enter regulators analogous to $G_{\pi N}$, but that the

resulting predictions for $F_2^{c\bar{c}}$ at the upper reaches of the Q^2 of measurements recorded by the European Muon Collaboration (EMC) [6] were rather large. As these measurements have been cited as evidence of IC [7], a more systematic analysis of the model developed in [1] using the technology of a QCD global fit is especially timely. Moreover, a thorough global analysis would also be capable of assessing the impact of the suggestive EMC data in a setting that comprehensively allows IC.

Such an effort has recently been carried out and described in Ref. [8]; for this purpose, it was convenient to fit the models in [1] to simple, three-parameter expressions of the form

$$c(x) = C^{(0)} A x^\alpha (1-x)^\beta, \quad \bar{c}(x) = C^{(0)} \bar{A} x^{\bar{\alpha}} (1-x)^{\bar{\beta}}, \quad (10)$$

where the normalization constants are defined in terms of beta functions as $A = 1/B(\alpha + 1, \beta + 1)$ and $\bar{A} = 1/B(\bar{\alpha} + 1, \bar{\beta} + 1)$, so as to enforce the normalization of the distributions to $C^{(0)}$. The overall normalization $C^{(0)}$ in Eq. (10) is then directly related to the total momentum carried by IC, given by

$$\langle x \rangle_{\text{IC}} = \int_0^1 dx x \{c + \bar{c}\}(x); \quad (11)$$

and one can collectively fit the world data involving various reactions over a wide kinematical range.

The QCD global fit was performed using the JR14 framework developed in Ref. [9], which among other things provides a sensitive treatment of finite- Q^2 corrections due to higher twist and target/quark mass effects. We are thus enabled to incorporate data with less restrictive cuts in W^2 and Q^2 as compared with previous efforts, *e.g.*, [10], that allowed a significant IC component to the nucleon. For the sake of the analysis, the F_2 structure function is assumed to be a combination of light and heavy contributions $F_2 = F_2^{\text{light}} + F_2^{\text{heavy}}$, in which F_2^{light} represents the (u, d, s) light-sector piece, whereas F_2^{heavy} contains the heavy c and b quarks. The charm-sector component of F_2^{heavy} may be further broken into a part which is generated through pQCD-calculable processes, $F_2^{c\bar{c}}$, as well as an intrinsic part, F_2^{IC} ; *i.e.*, $F_2^c = F_2^{c\bar{c}} + F_2^{\text{IC}}$. The pQCD component $F_2^{c\bar{c}}$ at intermediate Q^2 is described by the photon-gluon fusion mechanism computed formally in Ref. [11]; in particular, calculating the necessary diagrams to NLO in α_s yields

$$F_2^{c\bar{c}}(x, Q^2, m_c^2) = \frac{Q^2 \alpha_s}{4\pi^2 m_c^2} \sum_i \int \frac{dz}{z} \hat{\sigma}_i(\eta, \xi) f_i\left(\frac{x}{z}, \mu\right), \quad (12)$$

with $\hat{\sigma}_i$ denoting the hard, parton-level scattering of a flavor $i = u, d, s$ or g into final states consisting of a $c\bar{c}$ pair. On the other hand, f_i represents the associated parton densities in the nucleon.

The Hoffmann-Moore scheme of [11] systematically incorporates mass-dependent threshold effects, and $\hat{\sigma}_i$ must therefore be computed in terms of the parameters $\xi = Q^2/m_c^2$ and $\eta = Q^2 \cdot (1-z)/(4m_c^2 z) - 1$; additionally, the parton densities of Eq. (12) must also be evaluated at a factorization scale specified by $\mu_F^2 = 4m_c^2 + Q^2$, in which we take the charm mass to be $m_c = 1.3$ GeV at threshold for consistency with the ‘confining’ prescription of [1]. We point out also that the present analysis assumed a partonic threshold $W^2 > (2m_c)^2$ in evaluating F_2^c . Relating this condition to the correspondingly larger hadronic threshold for the production of charm-containing final states is generally model-dependent, but has been undertaken in Ref. [8]. It should be noted that hadronic threshold effects can potentially impose more restrictive kinematical cuts on the data involved, and therefore slightly weaken the sharp growths in χ^2 presented below.

Of the data we incorporate at lower Q^2 and W^2 , ep and ed fixed-target DIS measurements [12] from SLAC are especially influential in limiting the magnitude of $\langle x \rangle_{\text{IC}}$, as we explore in Fig. 3. In both panels of Fig. 3, we plot the rise in χ^2 against the magnitude of $\langle x \rangle_{\text{IC}}$ assumed in the IC model parametrized according to Eq. (10). Moreover, we globally fit data in this fashion twice — excluding and actively including the EMC extractions of F_2^c as shown in the left and right panels of Fig. 3, respectively. The results of this procedure are striking: the rapid takeoff of χ^2 from $\langle x \rangle_{\text{IC}} \sim 0$ indicates plainly that the world data sharply limit the size of IC, with the SLAC measurements serving as a principal constraint (as illustrated by the ‘scans,’ which explicitly separate the contributions to the growth of χ^2). In fact, the ‘total’ fit of the LHS of Fig. 3 amounts to a 5σ limit of $\langle x \rangle_{\text{IC}} \leq 0.1\%$.

In the end, inclusion of the EMC points of Ref. [6] does little to soften this restrictive bound — while the scan corresponding to the EMC set (green dot-dashed) in the right panel of Fig. 3 exhibits a minimum in χ^2 about $\langle x \rangle_{\text{IC}} \sim 0.3 - 0.4\%$, this shallows significantly when combined with the global

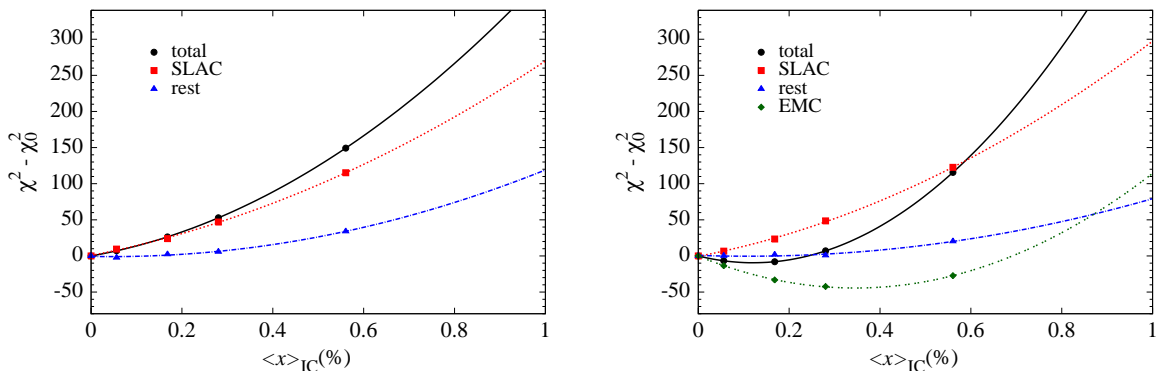


Fig. 3 Dependence on $\langle x \rangle_{IC}$ of the χ^2 of fits that omit (left) and incorporate (right) the EMC $F_2^{c\bar{c}}$ data.

data; the ‘total’ fit in this case prefers $\langle x \rangle_{IC} = 0.13 \pm 0.04\%$. In Ref. [8] we noted that the EMC data themselves exhibit some degree of tension with other segments of the data sets we fit, most notably, HERA measurements of the reduced charm cross section $\sigma_r^{c\bar{c}}$ [13]. Specifically, these data occupy partially overlapping regions of the kinematical parameter space with respect to the older EMC measurements, but are comparably much better fit by the global analysis (unlike the EMC points, which have $\chi^2/n_{d.o.f.} \sim 4.3$). Evidence of such tension in data that weigh critically in favor of IC should do nothing but urge the necessity of new and improved measurements of charm production, especially at large x .

Acknowledgements The author acknowledges J. T. Londergan, W. Melnitchouk, C. E. Keppel, B. Wojtsekhowski, and P. Jimenez-Delgado for collaboration on projects related to this note, as well as G. A. Miller for helpful discussions. The author also gratefully acknowledges support from the Gary T. McCartor Fund Fellowship.

References

1. T. J. Hobbs, J. T. Londergan and W. Melnitchouk (2014) *Phenomenology of nonperturbative charm in the nucleon*. Phys. Rev. D **89**, 074008
2. A. W. Thomas (1983) *A Limit on the Pionic Component of the Nucleon Through SU(3) Flavor Breaking in the Sea*. Phys. Lett. B **126**, 97
3. A. Camsonne, et al. (2014) *Measurement of Tagged Deep Inelastic Scattering (TDIS)*. Jefferson Lab Proposal PR12-14-010
4. H. Holtmann, A. Szczurek and J. Speth (1996) *Flavor and spin of the proton and the meson cloud*. Nucl. Phys. A **596**, 631
5. S. J. Brodsky, P. Hoyer, C. Peterson and N. Sakai (1980) *The Intrinsic Charm of the Proton*. Phys. Lett. B **93**, 451
6. J. J. Aubert *et al.* [European Muon Collaboration] (1983) *Production of charmed particles in 250-GeV μ^+ - iron interactions*. Nucl. Phys. B **213**, 31
7. S. J. Brodsky, B. Kopeliovich, I. Schmidt and J. Soffer (2006) *Diffractive Higgs production from intrinsic heavy flavors in the proton*. Phys. Rev. D **73**, 113005
8. P. Jimenez-Delgado, T. J. Hobbs, J. T. Londergan and W. Melnitchouk, *New limits on intrinsic charm in the nucleon from global analysis of parton distributions*. Phys. Rev. Lett. **114**, no. 8, 082002 (2015)
9. P. Jimenez-Delgado and E. Reya (2014) *Delineating parton distributions and the strong coupling*. Phys. Rev. D **89**, 074049
10. S. Dulat, T. J. Hou, J. Gao, J. Huston, J. Pumplin, C. Schmidt, D. Stump and C.-P. Yuan (2014) *Intrinsic Charm Parton Distribution Functions from CTEQ-TEA Global Analysis*. Phys. Rev. D **89**, 073004
11. E. Hoffmann and R. Moore (1983) *Subleading Contributions to the Intrinsic Charm of the Nucleon*. Z. Phys. C **20**, 71
12. L. W. Whitlow, E. M. Riordan, S. Dasu, S. Rock and A. Bodek (1992) *Precise measurements of the proton and deuteron structure functions from a global analysis of the SLAC deep inelastic electron scattering cross-sections*. Phys. Lett. B **282**, 475
13. H. Abramowicz *et al.* [H1 and ZEUS Collaborations] (2013) *Combination and QCD Analysis of Charm Production Cross Section Measurements in Deep-Inelastic ep Scattering at HERA*. Eur. Phys. J. C **73**, 2311